HHS Public Access

Author manuscript

Breast Cancer Res Treat. Author manuscript; available in PMC 2015 March 18.

Published in final edited form as:

Breast Cancer Res Treat. 2014 February ; 144(1): 93–101. doi:10.1007/s10549-014-2854-5.

Ex vivo Evans blue assessment of the blood brain barrier in three breast cancer brain metastasis models

John Do,
Department of Surgery, Stanford University School of Medicine, Stanford, CA 94305, USA

Deshka Foster,
Department of Surgery, Stanford University School of Medicine, Stanford, CA 94305, USA

Corinne Renier,
Department of Surgery, Stanford University School of Medicine, Stanford, CA 94305, USA

Hannes Vogel,
Department of Pathology, Stanford University School of Medicine, Stanford, CA, USA

Sahar Rosenblum,
Department of Neurosurgery, Stanford University School of Medicine, Stanford, CA, USA

Timothy C. Doyle,
Department of Pediatrics, Stanford University School of Medicine, Stanford, CA, USA

Victor Tse, and
Department of Neurosurgery, Stanford University School of Medicine, Stanford, CA, USA

Irene Wapnir
Department of Surgery, Stanford University School of Medicine, Stanford, CA 94305, USA

Irene Wapnir: wapnir@stanford.edu

Abstract

The limited entry of anticancer drugs into the central nervous system represents a special therapeutic challenge for patients with brain metastases and is primarily due to the blood brain barrier (BBB). Albumin-bound Evans blue (EB) dye is too large to cross the BBB but can grossly stain tissue blue when the BBB is disrupted. The course of tumor development and the integrity of the BBB were studied in three preclinical breast cancer brain metastasis (BCBM) models. A luciferase-transduced braintropic clone of MDA-231 cell line was used. Nude mice were subjected to stereotactic intracerebral inoculation, mammary fat pad-derived tumor fragment implantation, or carotid artery injections. EB was injected 30 min prior to euthanasia at various timepoints for each of the BCBM model animals. Serial bioluminescent imaging demonstrated exponential tumor growth in all models. Carotid BCBM appeared as diffuse multifocal cell clusters. EB aided the localization of metastases ex vivo. Tumor implants stained blue at 7 days whereas gross staining was not evident until day 14 in the stereotactic model and day 28 for the carotid model. EB

Correspondence to: Irene Wapnir, wapnir@stanford.edu.

John Do and Deshka Foster have contributed equally to this study.

assessment of the integrity of the BBB provides useful information relevant to drug testing in preclinical BCBM models.

Keywords

Breast cancer brain metastasis; Mouse brain metastasis model; Blood brain barrier

Introduction

An increasing number of women with breast cancer develop brain metastases with disease progression, either as a site of first failure or accompanying extracranial metastatic disease [1–6]. Triple negative and HER2 overexpressing cancers are disproportionately represented [7–10]. However, new patterns are emerging in the case of HER2 positive breast cancers treated adjuvantly with trastuzumab. This has led to a dramatic drop in the number of patients developing non-central nervous system (CNS) metastases in addition to a relative increase in the incidence of brain metastases and the proportion of patients with brain as first site of recurrence [6, 11]. The limited access of many anticancer drugs to the CNS poses a special therapeutic challenge for patients who develop brain metastases. Supratentorial parenchymal lesions are the most common sites of CNS metastases occurring in the watershed vascular regions of the brain, while leptomeningeal metastases comprise less than 20 %of cases [11–13]. Surgical resection and/or brain radiotherapy are the most effective interventions available. Chemotherapy in general has poor or limited penetrance in the brain, but newer targeted agents are associated with more promising outcomes [2, 14].

The blood brain barrier (BBB) is believed to represent a major impediment to the effective delivery of many anticancer drugs to the CNS in spite of the fact that the tumor-associated vasculature is more permeable [1]. At the cellular level, the BBB consists of a capillary endothelium lacking fenestrations and connected via tight junctions [15]. Additionally, efflux transport proteins localized on the endothelium further diminish the effectiveness of circulating drugs [16]. It is widely believed that modification of the BBB is initiated, as tumor cells proliferate in the brain. As permeability increases, the entry of drugs to the brain improves, although the data documenting this phenomenon are sparse [17].

Experimental breast cancer brain metastasis (BCBM) models can be technically challenging but play an important role in the study of metastasis and testing of new treatments. Hematogenous-derived brain metastases have been most successfully reproduced using intra-cardiac or carotid artery injections with only a few human breast cancer cell lines, specifically a braintropic clone of MDA-MB-231 and HER2-transfected MCF-7 cells [5, 18, 19]. Cardiac and carotid injections require special expertise including ultrasound guidance for the former and microscopic dissection for the latter [19–21]. In contrast, tumor fragment implantation and stereotactic injection models are easier to execute and better tolerated by the animals.

From an experimental viewpoint, ascertaining the status of the BBB in brain metastasis animal models is useful for the interpretation of drug therapies in the CNS and where the rate-limiting step may be the BBB. A relatively simple way to assess BBB permeability is

with the use of a detectable agent too large to cross an intact BBB. Evans blue (EB) dye binds to albumin forming a 68 kDa complex, which cannot cross an intact BBB and, thus, cannot enter the CNS [22–24]. Alternatively, when the BBB is disrupted, the adjacent tissue will stain blue. We describe here the anatomic integrity of BBB in BCBM models. Each model can theoretically simulate clinical scenarios and thus may be useful in preclinical studies of brain metastases treatments.

Materials and methods

Three BCBM mouse models were developed using a brain-tropic clone of the human ER, PR, and HER2 negative MDA-MB-231 breast cancer cell line (kindly provided by Dr. Yoneda of University of Texas Health Science Center at San Antonio, TX, USA). Moreover, this cell line was transduced with two reporter genes, one gene encoding for the sodium iodide symporter (NIS) gene under an internal CMV promoter and linked bicistronically to the firefly luciferase (luc) gene. Once transduced, single cell colonies isolated by limiting dilution cells were screened in vitro for luc activity and were selected for the highest bioluminescent signal. Cells were maintained with limited passaging in RPMI medium with 10 % fetal bovine serum and 1 % penicillin and streptomycin. Prior to animal injection, cells were cultured until 70 % confluent and re-suspended in phosphate-buffered solution.

Animal experiments

All animal experiments were conducted under the approval of the Administrative Panel on Laboratory Animal Care (APLAC) at Stanford University. Female Ncr-nu nude mice (5–8 weeks old; Taconic, Oxnard, CA, USA) were used. Mice were anesthetized with continuous 2–3 % isoflurane via a nose cone for all experiments except the stereotactic model whereby the anchoring of the mice does not permit the administration of anesthetic gas.

Stereotactic intracranial injection of tumor cells

Mice were anesthetized with ketamine (100 mg/kg) and xylazine (10 mg/kg) solution IP and placed prone on a stereotactic frame (David Kopf Instruments, Tujunga, CA, USA). A 0.5-mm burr hole, 2-mm lateral, and 2-mm posterior to the bregma were made using an F.S.T. High Speed Micro-Drill and a carbon steel burr tip under a dissecting microscope (Seiler Precision Microscopes, St. Louis, MO, USA). Following dural penetration, a 5 μl 26-gauge fixed-needle microinjector syringe (Hamilton Microliter™ #75, Hamilton Co, Reno, NV, USA) was inserted 2.5-mm deep into the region of the basal ganglia. A 2 μl cell suspension containing $2–3 \times 10^5$ tumor cells was delivered over a period of 5 min (Fig. 1a). The needle was then retracted over a 5-min period. The burr hole was then sealed with bone wax and the scalp sutured. Mice were weighed and imaged serially on a biweekly basis to monitor bioluminescent tumor development.

Intracranial implantation of mammary fat-pad (MFP) xenografts

Continuous isoflurane (2–3 %) anesthesia was used for all the experiments. Orthotopic tumor xenografts were developed in the MFP with 2.5×10^6 cells suspended in Matrigel (BD Biosciences, San Jose, CA, USA). Intracranial tumor transplantation was performed once MFP tumors had achieved a diameter greater than 7 mm (about 2 weeks post-

injection). Mice were injected with luciferin IP 15 min before MFP tumors were excised and minced into 1-mm^3 fragments (Fig. 2a). These pieces were imaged ex vivo to identify the most bioluminescent fragments for transplant. A 1-mm burr hole was made at the same anatomic location described above for stereotactic inoculation. The dural surface was disrupted, and the tumor fragment was gently inserted into brain parenchyma. The burr hole was sealed using bone wax, and the scalp was sutured. Mice were weighed and serially imaged on a biweekly basis as previously described.

Carotid injection

Mice were anesthetized as previously described for intracranial implantation. A vertical incision was made from below the hyoid bone toward the sternal notch. Tissue antero-lateral to the trachea was bluntly dissected, and the strap muscles were swept laterally (Fig. 3a). A 33 gage Hamilton needle attached to a 10 μl Hamilton micro-injector syringe was used to inject a suspension of 2.5–7.5 × 10^4 cells in a volume of 5 μl PBS into the left common carotid artery (CCA) just proximal to the bifurcation, with or without occlusion of external carotid artery (ECA). Gentle pressure with absorbable gelatin sponge (Surgifoam U.S.P, Ethicon) was applied to control needlepoint bleeding. The skin was re-approximated with 6-0 silk interrupted sutures. Mice were weighed on a biweekly basis and judiciously hydrated on a daily basis with subcutaneous saline during the first post-procedure week.

In vivo bioluminescent imaging

Mice were serially imaged at day 4 or 5 post-injection in the stereotactic and implant models and then continued twice per week, until mice were euthanized. Carotid injection mice were not imaged until day 10. Luciferin (150 mg/kg mouse; Biosynth International Inc, Itasca, IL, USA) was injected IP and anesthetized with isoflurane (2–3 %). Imaging was performed with a cooled charge-coupled device camera system (IVIS Imaging System 100; Caliper Life Sciences, Hopkinton, M, USA). Animals were imaged with 30-s exposures every 3 min, until the peak value of bioluminescent flux (photons/second) was observed. Bioluminescence was analyzed using Living Image software (version 4.3; Caliper Life Sciences, Hopkinton, MA, USA). The same region of interest (ROI) was applied sequentially and for all mice. ROI was also measured for background bioluminescence for each mouse. Successful tumor generation was defined by bioluminescence for signals greater than background flux (10^5 p/s).

Three-dimensional BLI (IVIS-Spectrum; Xenogen/Caliper Life Sciences) and computer tomography (CT) scans (Flex-SPECT-CT; Gamma Medica Ideas/TriFoil Imaging, Northridge, CA, USA) were performed on representative animals from each of the BCBM models. CT with BLI overlay data generated tumor localization in the brain, which was analyzed with Living Image 3D (Caliper Life Science) and GEHC Microview (GE Healthcare) software.

BBB integrity

EB staining was studied at various timepoints for each of the BCBM model animals. Time intervals from implantation or injection to tumor development differed from one model to the next. Solution of 2 % EB was injected (4 ml/kg) via the femoral vein in anesthetized

animals and allowed to circulate for 30 min [24]. Deeply anesthetized mice were perfused with physiological saline to wash out excess EB and then euthanized. Brains were extracted and placed in 10 % neutral buffered formalin prior to processing and sectioning. EB staining was photographically recorded. Following sectioning, slides were placed in xylene for 30 min prior to mounting. EB penetration through the BBB was further assessed by fluorescent microscopy (Nikon Eclipse 80i).

Histology and immunohistochemistry

Formalin-fixed tissues were embedded in paraffin, and 5 μm coronal sections were stained with hematoxylin and eosin (H&E). To identify human tumor cells in the brain parenchyma, representative sections were stained with monoclonal anti-HLA Class 1 ABC antibody (clone EMR8-5, Abcam Inc., Cambridge, MA, USA). Microscopic images were viewed (Nikon Microscope 80i) and obtained on a mounted digital camera (Nikon Digital Camera DXM1200F).

Results

Stereotactic injection of tumor cells was the quickest method, taking approximately 20 min, and resulting in the shortest time to develop brain metastasis (Fig. 1). The major disadvantage of stereotactic injection is the setup, which requires immobilizing the head of the mouse in the stereotactic frame. Slight variation in the depth and angle of the needle can lead to injection of cells in the ventricular system and tracking of cells along the needle track. Transplantation of MFP tumor fragments was technically easy to accomplish, each procedure requiring approximately 30 min and resulting in a high yield of brain metastasis. However, MFP xenografts must first be generated, which add approximately two weeks to the procedure (Fig. 2). Carotid artery model was the most technically challenging, requiring extensive practice to master the microsurgical dissection and slow injection of a cell suspension into the CCA (Fig. 3).

Tumor development

Stereotactic model—The pattern of tumor development for 18 mice injected with 2 or 3 $\times 10^5$ cells is shown over 28-day period. A CT scan with BLI overlay on day 25 illustrates the intracerebral location of generated metastasis in this model (Fig. 1b). No weight loss, neurologic, or behavioral changes were noted. Average bioluminescence (flux) of serially imaged mice exhibited exponential growth on days 4–25 ($R^2 = 0.998$) (Fig. 1c). Tumors developed in 15 (83 %) mice by the end of the first week, with bioluminescent signals greater than 1×10^5 p/s. Of ten mice imaged on days 4 and 7, three demonstrated up to 49 % transient decrease in bioluminescence during this time interval. Subsequently, there was dramatic growth corresponding to more than a 100-fold increase on average in bioluminescence. In some mice, more than one area of focal BLI was observed, which we presume resulted from inadvertent injection of tumor cells into the ventricular system of seeding along the needle track.

Two mice at each timepoint were perfused with EB at post-injection days 7, 10, and 14 (Fig. 4). While for days 15, 28, 35, and 49, one animal at each timepoint was injected. Tumors

were histologically identified in 9 of 10 animals studied with EB in the stereotactic group. Microscopic detection of tumor cells correlated well with BLI. Stained tumors were visible on gross sectioning from mice sacrificed days 14–35 (Fig. 1d). Prior to day 14, EB staining was not observed, although isolated tumor cells or cell clusters were present on histologic sections. By day 28, most tumors measured close to 3 mm in the longest diameter. Tumor-specific EB staining was confirmed by microscopic fluorescence analysis in this model as shown in Fig. 1e.

Implantation model—A total of nine mice were implanted with tumor fragments, and none of these mice experienced weight loss. CT scan imaging with BLI overlay confirms the superficial location of embedded tumor (Fig. 2b). A lag phase in tumor growth was noted in 57 % of cases, associated with a 95 % decrease in signal on day 7 compared to day 4. However, average tumor bioluminescence showed exponential increase in tumor signal from post-implantation day 5 through day 35 ($R^2 = 0.958$) as shown in Fig. 2c. Bioluminescent signals greater than 1×10^5 p/s were evident within 7 days post-injection for 5 of 9 mice with implanted. By day 21, there was a mean 100-fold increase in bioluminescence, and exponential growth continued through day 35.

Implanted tumors demonstrated infiltration into the brain parenchyma on gross examination and were adherent to the dura and skull. EB experiments were performed on a total of 4 animals at days 7, 35 (2), and 56 post-implantation. Tumor-specific EB staining was consistently identified at all timepoints. Histological confirmation of tumor formation also coincided with high bioluminescence (Figs. 2d, 4).

Carotid artery injections—A total of 29 mice were subjected to carotid injections with $5–7.5 \times 10^4$ cells. Mice ($n = 4$) injected with a lower concentration of cells, 2.5×10^4, revealed no bioluminescence after a 42-day period. Ligation of the ECA in ten mice did not improve the rate of tumor formation with 5×10^4 cells. Carotid injection with 5×10^4 cells showed comparable tumor development to 7.5×10^4 cells ($n = 4$). There were three intraoperative deaths due to hemorrhage and three additional deaths within 7 days of the procedure. Dramatic weight loss of up to 21.7 % body weight was observed in these mice over the first week, in spite of undergoing daily subcutaneous saline injections to ensure hydration.

Tumors developed in 19 of 23 (83 %) over 42 days post-injection as detected by BLI, exhibiting exponential growth ($R^2 = 0.979$) between post-injection days 14 and 31 (Fig. 3c). Only 4 of 23 (17 %) mice had significant bioluminescence signals of 1×10^5 p/s or more at 14 days post-injection. By day 20, the mean bioluminescence for the group increased tenfold to 1×10^6 p/s and 100-fold in 32 % of mice followed over 28 days. CT with BLI overlay was not informative in most carotid injection cases with the exception of a unique case exhibiting a well-localized macrometastasis as shown in Fig. 3b.

Nine mice were sacrificed 14, 17, 22, 27, 28, 41, 42, and 59 days post-injection. EB staining of brain tissue was faint and diffuse in specimens examined through day 27 (Fig. 3d). Gross examination of excised brains revealed visible tumors in only two instances. Histologically, tiny clusters of single, compressed-appearing tumor cells were identified from post-injection

day 14–27. BLI increased to 10^7 p/s range or more than 200 times background signal after day 28. Localized punctate areas of blue staining were more apparent, correlating with microscopic identifiable tumor cells (Figs. 3d, 4). The anatomic distribution of blue staining was quite variable involving forebrain, midbrain, occipital lobes, and cerebellum.

Fluorescent microscopy

BBB permeability was further characterized by fluorescence microscopy in the stereotactic model. Correlation among tumor histology, blue staining of gross tumors and microscopic fluorescence were demonstrated. Figure 1e depicts an H&E section of a 28-day brain metastasis. A parallel section and dark-field photography demonstrate tumor cell specific fluorescence.

Discussion

The brain is a unique sanctuary, characterized by the presence of the BBB [1]. In this study, disruption of the BBB was demonstrated in all three MDA-231-Br BCBM models studied. BLI proved to be a reliable indicator of developing tumors while EB revealed the anatomic location of metastases when the integrity of the BBB was compromised. At early experimental timepoints in stereotactic and carotid injected models, low bioluminescence without EB staining was observed, suggesting that the BBB remains intact, when metastases are microscopic [25]. Specifically, 1 week after inoculation in the stereotactic model, tumor cell clusters measured less than 0.5 mm, and no EB staining was detected. Similarly, after carotid artery injection, EB staining was absent during the first 4 weeks. This is consistent with histologic findings of isolated cells or cell clusters localized along microvessels, as described by Lorger and Felding-Habermann [18]. The decrease in BLI observed after stereotactic cell injection or tumor fragment implantation also suggests that many cells do not survive the initial steps of tumor development in the brain microenvironment [18]. It follows from these results that if anticancer drugs were administered during this early phase of BCBM development, cells would be readily shielded from the toxic effects of circulating agents by an intact BBB [5]. Indeed, this may be the scenario for patients with early-stage breast cancer, who harbor occult, subclinical brain metastases and whose systemic therapies fail to penetrate the BBB and CNS.

Luciferin easily crosses the BBB and is readily metabolized by tumor cells providing a suitable non-invasive measure for tumor cell proliferation [26]. As tumors grow, BLI correspondingly increases, and EB staining appears more distinct and intense, indicating loss of integrity in the BBB at the site of tumor formation. The pattern of EB staining in the carotid injection model, however, was diffuse corresponding to high BLI from multiple tiny tumor clusters through the brain parenchyma. Our studies using tumor fragments derived from MFP xenografts, showed intense EB staining even within the first week, suggesting that early contact with the subarachnoid vascular network facilitates the establishment of perfusion [27]. Intracranial implantation differs from the other brain metastases models, because it is partially, if not completely, supplied by branches of the ECA or systemic vasculature. This model may approximate leptomeningeal involvement in the clinical setting with the caveat that MFP-derived implants contain an admixture of epithelial and stromal

cells [13]. Contrastingly, the carotid and stereotactic models develop exclusively from epithelial tumor cell inoculations. Surprisingly, in some instances, inoculated cells by stereotactic injection gave rise to tumors away from the injection sites, including the development of spinal metastasis viewed by BLI (not presented here). One plausible explanation is the inadvertent injection of cells into the lateral ventricle or tracking of cells along the trajectory of the needle. The limited entry of anticancer drugs into the CNS represents a special therapeutic challenge for patients with brain metastases [5]. Experimental BCBM models are technically challenging, but such models are important for preclinical drug testing [28]. Therefore, therapeutic efficacy should be linked to the assessment of the BBB. Each model attempts to mimic clinical scenarios occurring in patients with predominant parenchymal BCBM, while the fragment implantation method may more closely recapitulate leptomeningeal involvement [13, 27, 29]. Typically brain metastases appear with disease progression and are discovered, once BBB permeability has been altered [2]. The demand for adjuvant treatments that cross the CNS will certainly increase in the future. Influx and efflux transporters, together with the BBB, are important determinants of effective drug delivery [30]. The evaluation of any agent for the treatment of BCBM in experimental murine models should be judged in the context of the BBB. In turn, this may provide useful information for patients with brain metastases.

Based on our findings, EB dye is as a simple and practical method to evaluate the status of the BBB which may be crucial to the timing of experimental studies involving drug delivery to brain metastasis. While magnetic resonance imaging (MRI) is also capable of evaluating BBB integrity [25, 31, 32], EB represents a straightforward and inexpensive method. In summary, the utility of EB perfusion prior to animal sacrifice in experimental brain metastasis models serves to determine the status of the BBB and can aid the ex vivo localization of tumors within mouse brain parenchyma.

Acknowledgments

We would like to thank Dr. Sanjiv Sam Gambhir for his technical support. This study was supported in part by the Komen for the Cure grant (KG090545), Small Animal Imaging Resource NIH-NCI ICMIC P50-CA114747-02 (Gambhir, PI), and Stanford University Cancer Center NIH NCI CCSG P30-CA124435-02 (Mitchell, PI).

References

1. Aragon-Ching JB, Zujewski JA. CNS metastasis: an old problem in a new guise. Clin Cancer Res. 2007; 13:1644–1647. [PubMed: 17363516]
2. Dawood S, Gonzalez-Angulo AM. Progress in the biological understanding and management of breast cancer-associated central nervous system metastases. Oncologist. 2013; 18:675–684. [PubMed: 23740934]
3. Minisini A, Moroso S, Gerratana L, Giangreco M, Iacono D, Poletto E, Guardascione M, Fontanella C, Fasola G, Puglisi F. Risk factors and survival outcomes in patients with brain metastases from breast cancer. Clin Exp Metastasis. 2013
4. Lin NU, Claus E, Sohl J, Razzak A, Arnaout A, Winer E. Sites of distant relapse and clinical outcomes in patients with metastatic triple-negative breast cancer: high incidence of central nervous system metastases. Cancer. 2010; 113:2638–2645. [PubMed: 18833576]
5. Gril B, Evans L, Palmieri D, Steeg PS. Translational research in brain metastasis is identifying molecular pathways that may lead to the development of new therapeutic strategies. Eur J Cancer. 2010; 46:1204–1210. [PubMed: 20303257]

6. Olson EM, Abdel-Rasoul M, Maly J, Wu CS, Lin NU, Shapiro CL. Incidence and risk of central nervous system metastases as site of first recurrence in patients with HER2-positive breast cancer treated with adjuvant trastuzumab. Ann Oncol. 2013; 24:1526–1533. [PubMed: 23463626]
7. Hicks DG, Short SM, Prescott NL, Tarr SM, Coleman KA, Yoder BJ, Crowe JP, Choueiri TK, Dawson AE, Budd T, Tubbs RR, Casey G, Weil RJ. Breast cancers with brain metastases are more likely to be estrogen receptor negative, express the basal cytokeratin CK5/6, and overexpress HER2 or EGFR. Am J Surg Pathol. 2006; 30:1097–1104. [PubMed: 16931954]
8. Slimane K, Andre F, Delaloge S, Dunant A, Perez A, Grenier J, Massard C, Spielmann M. Risk factors for brain relapse in patients with metastatic breast cancer. Ann Oncol. 2004; 15:1640–1644. [PubMed: 15520065]
9. Miller KD. Occult central nervous system involvement in patients with metastatic breast cancer: prevalence, predictive factors and impact on overall survival. Ann Oncol. 2003; 14:1072–1077. [PubMed: 12853349]
10. Clark GM, Sledge GW, Osborne CK, McGuire WL. Survival from first recurrence: relative importance of prognostic factors in 1,015 breast cancer patients. J Clin Oncol. 1987; 5:55–61. [PubMed: 3806159]
11. Hwang TL, Close TP, Grego JM, Brannon WL, Gonzales F. Predilection of brain metastasis in gray and white matter junction and vascular border zones. Cancer. 1996; 77:1551–1555. [PubMed: 8608542]
12. Lin NU, Bellon JR, Winer EP. CNS metastases in breast cancer. J Clin Oncol. 2004; 22:3608–3617. [PubMed: 15337811]
13. Scott BJ, Kesari S. Leptomeningeal metastases in breast cancer. Am J Cancer Res. 2013; 3:117–126. [PubMed: 23593536]
14. Karam I, Lesperance MF, Berrang T, Speers C, Tyldesley S, Truong PT. pN0(i+) breast cancer: treatment patterns, locoregional recurrence, and survival outcomes. Int J Radiat Oncol Biol Phys. 2013; 87:731–737. [PubMed: 24035330]
15. Fidler IJ. The role of the organ microenvironment in brain metastasis. Semin Cancer Biol. 2011; 21:107–112. [PubMed: 21167939]
16. Abbott NJ, Patabendige AA, Dolman DE, Yusof SR, Begley DJ. Structure and function of the blood–brain barrier. Neurobiol Dis. 2010; 37:13–25. [PubMed: 19664713]
17. Palmieri D, Chambers AF, Felding-Habermann B, Huang S, Steeg PS. The biology of metastasis to a sanctuary site. Clin Cancer Res. 2007; 13:1656–1662. [PubMed: 17363518]
18. Lorger M, Felding-Habermann B. Capturing changes in the brain microenvironment during initial steps of breast cancer brain metastasis. Am J Pathol. 2010; 176:2958–2971. [PubMed: 20382702]
19. Schackert G, Fidler IJ. Development of in vivo models for studies of brain metastasis. Int J Cancer. 1988; 41:589–594. [PubMed: 3356491]
20. Balathasan L, Beech JS, Muschel RJ. Ultrasonography-guided intracardiac injection: an improvement for quantitative brain colonization assays. Am J Pathol. 2013; 183:26–34. [PubMed: 23665347]
21. Chua JY, Pendharkar AV, Wang N, Choi R, Andres RH, Gaeta X, Zhang J, Moseley ME, Guzman R. Intra-arterial injection of neural stem cells using a microneedle technique does not cause microembolic strokes. J Cereb Blood Flow Metab. 2011; 31:1263–1271. [PubMed: 21157474]
22. Rapoport SI, Fredericks WR, Ohno K, Pettigrew KD. Quantitative aspects of reversible osmotic opening of the blood–brain barrier. Am J Physiol. 1980; 238:R421–R431. [PubMed: 7377381]
23. Liu R, Martuza RL, Rabkin SD. Intracarotid delivery of oncolytic HSV vector G47 D to metastatic breast cancer in the brain. Gene Ther. 2005; 12:647–654. [PubMed: 15647762]
24. Mehmet, K.; Ahishali, B. Assessment of permeability in barrier type of endothelium in brain using tracers: Evans blue, sodium fluorescein, and horseradish peroxidase. In: Turksen, K., editor. Methods Mol Biol. Totowa: Humana Press; 2011. p. 369-382.
25. Lockman PR, Mittapalli RK, Taskar KS, Rudraraju V, Gril B, Bohn KA, Adkins CE, Roberts A, Thorsheim HR, Gaasch JA, Huang S, Palmieri D, Steeg PS, Smith QR. Heterogeneous blood-tumor barrier permeability determines drug efficacy in experimental brain metastases of breast cancer. Clin Cancer Res. 2010; 16:5664–5678. [PubMed: 20829328]

26. Inoue Y, Kiryu S, Watanabe M, Tojo A, Ohtomo K. Timing of imaging after D-luciferin injection affects the longitudinal assessment of tumor growth using in vivo bioluminescence imaging. Int J Biomed Imaging. 2010; 2010:7–12.

27. Nieuwenhuys, R.; Voogd, J.; Van Huijzen, C. The human central nervous system: a synopsis and atlas. Berlin: Springer; 2007.

28. Daphu I, Sundstrøm T, Horn S, Huszthy PC, Niclou SP, Sakariassen PO, Immervoll H, Miletic H, Bjerkvig R, Thorsen F. In vivo animal models for studying brain metastasis: value and limitations. Clin Exp Metastasis. 2013; 30:695–710. [PubMed: 23322381]

29. Berghoff A, Bago-Horvath Z, Ilhan-Mutlu A, Magerle M, Dieckmann K, Marosi C, Birner P, Widhalm G, Steger G, Zielinski C, Bartsch R, Preusser M. Brain-only metastatic breast cancer is a distinct clinical entity characterised by favourable median overall survival time and a high rate of long-term survivors. Br J Cancer. 2012; 107:1454–1458. [PubMed: 23047551]

30. Deeken JF, Löscher W. The blood–brain barrier and cancer: transporters, treatment, and Trojan horses. Clin Cancer Res. 2007; 13:1663–1674. [PubMed: 17363519]

31. Prabhu SS, Broaddus WC, Oveissi C, Berr SS, Gillies GT. Determination of intracranial tumor volumes in a rodent brain using magnetic resonance imaging, Evans blue, and histology: a comparative study. IEEE Trans Biomed Eng. 2000; 47:259–265. [PubMed: 10721633]

32. Zhou H, Chen M, Zhao D. Longitudinal MRI evaluation of intracranial development and vascular characteristics of breast cancer brain metastases in a mouse model. PLoS One. 2013; 8:1–11.

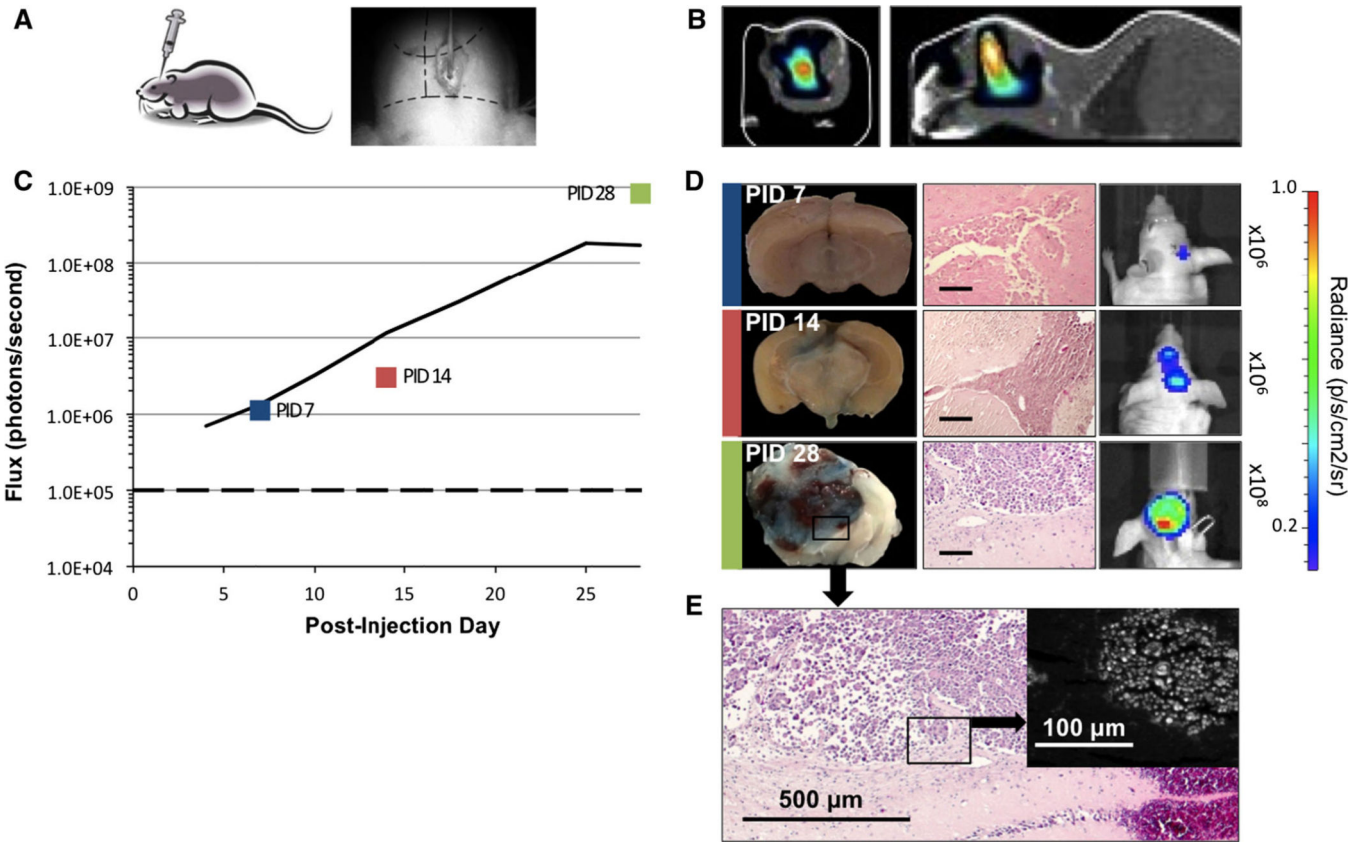

Fig. 1.

Brain metastases by stereotactic injection of MDA-231-Br cells. **a** Using a stereotactic frame, 2×10^5 cells are injected via a burr hole placed within 2 mm of the bregma (*right*). **b** CT scan with BLI overlay shows deep intracerebral signal on coronal and sagittal views. **c** In vivo average flux of 18 mice shows exponential ($R^2 = 0.998$) increase in bioluminescence over background (*dashed line*) days 4 through 25. **d** Whole brain coronal sections of mice PID 7, 14, 28 corresponding to color box datapoints in **c**. Evans blue staining of tumors is evident PID 14 and 28, indicating disruption of BBB; respective H&E sections (*scale bars* 100 µm) and in vivo mouse bioluminescent images. **e** Micrograph of PID 28 tumor shown in **d** with inset dark-field microscopy demonstrating fluorescence of cells stained by Evans blue

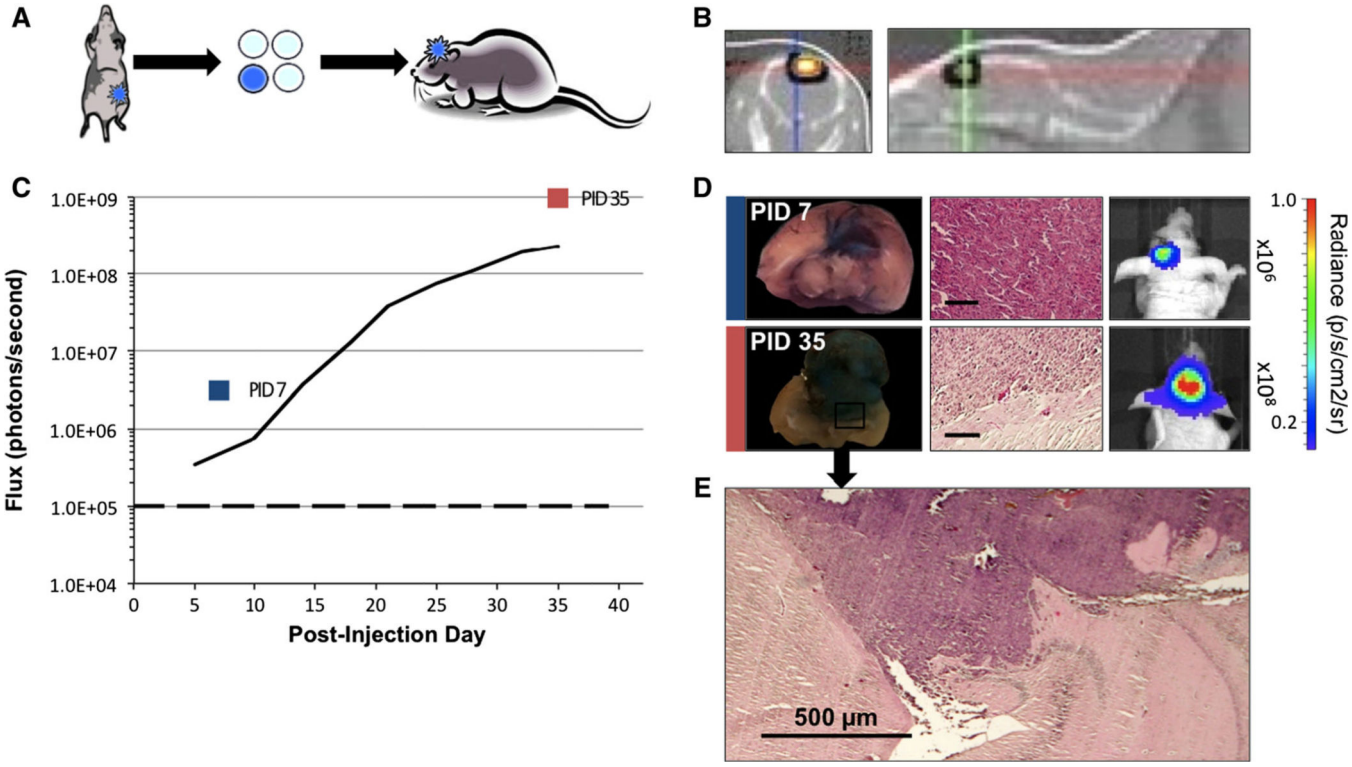

Fig. 2.

Brain metastases generated by implantation of MDA-231-Br tumor fragments. **a** Depiction of orthotopic MFP tumor (*left*), the selection of bioluminescent extracted fragment (*middle*), and implantation of 1 mm^3 fragments via burr hole into mouse brain (*right*). **b** CT scan imaging with BLI overlay shows intracerebral bioluminescent signal on coronal and sagittal views. **c** In vivo average flux of six mice BLI over a 35-day period shows (R^2 = 0.998) exponential increase in bioluminescence over background (*dashed line*) days 5–35. **d** Whole brain coronal sections of mice PID 7 and 35, corresponding to color box datapoints in **c**. Evans blue staining of tumors indicates disruption of the BBB. Parallel frames showing respective H&E sections (*scale bars* 100 µm) and in vivo mouse bioluminescent images. **e** Microphotograph of tumor invading brain parenchyma at PID 35 shown in **d**

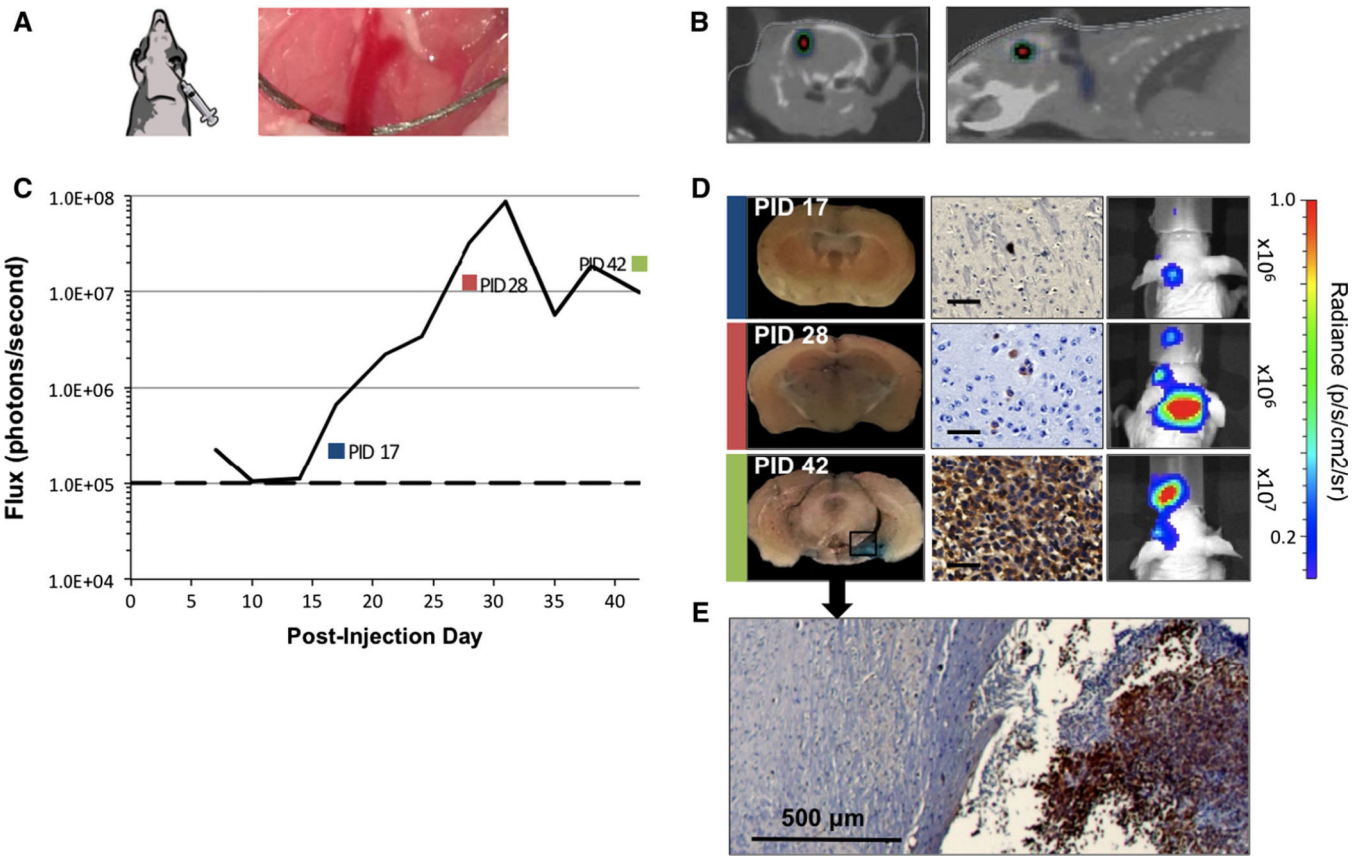

Fig. 3.

Brain metastases generated by CCA of MDA-231-Br cells. **a** Depiction of direct injection 5 × 10^4 cells into the CCA below the bifurcation into external and internal carotid branches (*right*). **b** CT scan with BLI overlay shows deep intracerebral bioluminescent signal on coronal and sagittal views. **c** In vivo average flux of 21 mice over first 42 days, showing exponential (R^2 = 0.979) increase in bioluminescence over background (*dashed line*) days 14 and 31. **d** Whole brain coronal sections of mice PID 17, 28, and 42, corresponding to color box datapoints in **c**. Evans blue staining was undetectable at 2 weeks but detectable by 4 weeks, indicating disruption of the BBB. Parallel frames show tumor cell reactivity to anti-HLA antibody (*scale bars* 100 µm) used to identify isolated cell clusters and corresponding mouse in vivo bioluminescence for specified time points. **e** Microscopic section of brain tumor-interface at PID 42 shown in **d**

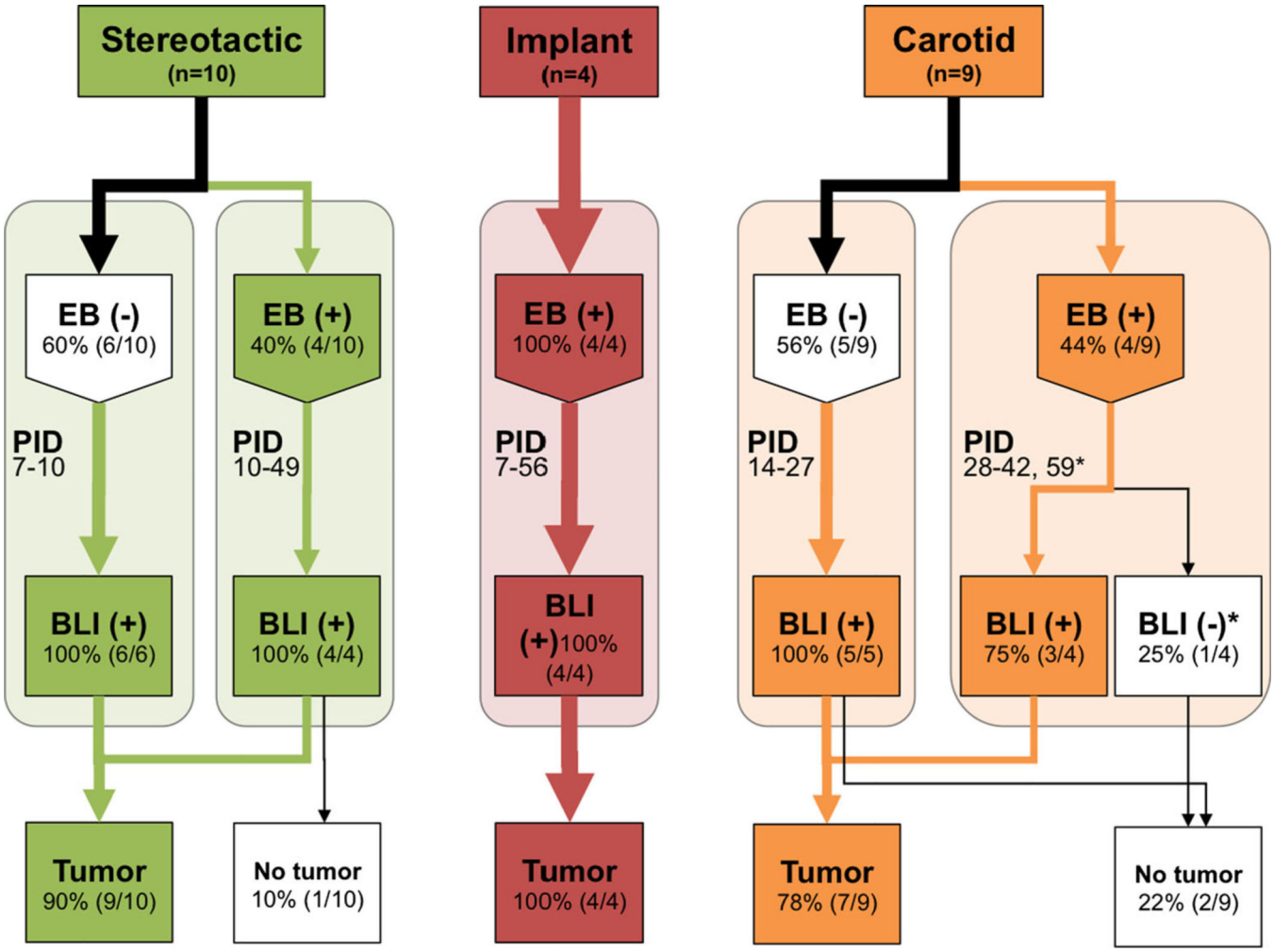

Fig. 4.

Evans blue, bioluminescence, and histology findings in three BCBM models. Flow chart of stereotactic (*green*), implant (*red*), and carotid (*orange*) models showing the proportion of mice with visible Evans blue staining at various time points and their corresponding bioluminescence (defined as greater than 1×10^5 p/s). Tumors were identified histologically with H&E (implant and stereotactic injection models) and anti-HLA staining (carotid injection model). *Mouse lost BLI signaling